Physica A 433 (2015) 9–16

Contents lists available at ScienceDirect

Physica A

journal homepage: www.elsevier.com/locate/physa

Phononic heat transfer through a one dimensional system subject to two sources of nonequilibrium

N. Beraha [a,b], A. Soba [b,c], R. Barreto [a,b], M.F. Carusela [a,b,*]

[a] Instituto de Ciencias, Universidad Nacional de Gral. Sarmiento, Los Polvorines, Argentina
[b] Consejo Nacional de Investigaciones Científicas y Técnicas, Buenos Aires, Argentina
[c] Centro de Simulación Computacional, Consejo Nacional de Investigaciones Científicas y Técnicas, Buenos Aires, Argentina

HIGHLIGHTS

- Energy transfer in systems subject to different sources of nonequilibrium is studied.
- Single and multiple resonant phenomena depending on the frequency regimes are found.
- A crossover between a mechanical resonance and a thermodynamical one is reported.
- A "red shift" resonance that is size dependent is shown.

ARTICLE INFO

Article history:
Received 14 November 2014
Received in revised form 16 March 2015
Available online 1 April 2015

Keywords:
Transport processes
Heat conduction
FK lattices

ABSTRACT

We analyze the energy transport in a one dimensional chain composed by two Frenkel–Kontorova (FK) segments connected together by a time modulated coupling. The ends are immersed in two thermal reservoirs with oscillating temperatures. We observe a single and multiresonant heat transport depending on the regimes considered, with a crossover between a mechanical resonance and a thermodynamical resonance. The dynamical tuning between these two regimes requires the synergetic presence of both time dependent sources of nonequilibrium. In the single resonant regime we analyze a "red shifted" resonant frequency that is dependent on the size of the system.

1. Introduction

During last years a fast development of the emerging field of *phononics* was achieved, where the manipulation and control of phonons (heat transfer) at the nanoscale and molecular level has become a fundamental topic due to its technological and practical implications [1]. The problem of phonon transport, that is a thermal nonequilibrium problem, is less understood than that of electron transport. In addition to electrons and photons, phonons carry heat and information. However, comparing with electron and photons, phonons are more difficult to control. So, an important and relevant issue is to understand further the mechanisms for heat transfer assisted by phonon and its generation in nano and micro devices and how it affects their structural stability. In this sense, it becomes essential to study mechanisms that dissipate or redirect heat efficiently, or under what operating conditions a given device can act as a good conductor or insulator.

It is known that two necessary conditions are fundamental for the emergence of thermal current: symmetry breaking and nonequilibrium sources. These two conditions in nonlinear lattices produce abnormal thermal transport phenomena, such as thermal rectification and negative differential thermal resistances.

* Corresponding author at: Instituto de Ciencias, Universidad Nacional de Gral. Sarmiento, Los Polvorines, Argentina.
E-mail address: flor@ungs.edu.ar (M.F. Carusela).

http://dx.doi.org/10.1016/j.physa.2015.03.024
0378-4371/

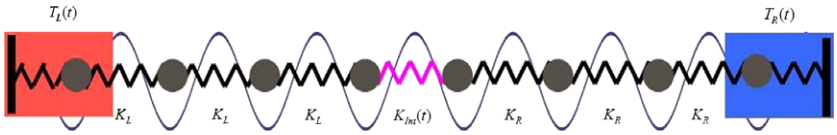

Fig. 1. Model system composed by two one-dimensional chains coupled by a modulated interaction in time and coupled to two heat baths Langevin at their ends.

Several models and mechanisms have been proposed to control or manipulate the heat at the nanoscale. One way is to tune the structural asymmetry or the degree of anharmonicity [2–11]. It has been demonstrated that the nonlinearity can be utilized to design novel nanoscale solid-state thermal devices such as thermal diodes [12–16], thermal transistors [17], thermal logic gates [18] and thermal memories [19,20].

Other mechanisms may require an external applied work on the system tuning or controlling heat *dynamically*. In Ref. [14] it was proposed a heat ratchet to direct heat flux from one bath to another in a nonlinear lattice, which periodically adjusts two baths temperatures while the average remains equal, or brownian heat motors to shuttle heat across the system [21]. We can also mention heat pumps which directs heat against thermal bias in nanomechanical systems [22], or phonon pumps induced at the molecular levels by an external force or with a mechanical switch on–off or a modulation of the coupling between different parts of the system [23–26]. Experimentally this can be done in molecular junctions or in molecular systems, for example, varying the distance among them. It was also demonstrate theoretically that mechanical actions as stretching (or compressing) a wire, can tuned the phononic band structure in such a way that multiple phononic channels are opened one by one. In this way and as in the electronic case, it is found a multiple-step quantized phononic thermal conductance [3].

The distinctive and unique transport properties of low-dimensional system has posted great challenge to find mechanisms to manipulate heat transfer in meso and nanoscopic phonon systems. Therefore, it is highly desirable any attempt towards a thorough understanding of the heat transport in general one-dimensional nonlinear lattice systems. In this paper we extend these studies to analyze the synergetic effect of heat transfer through one dimensional systems when are present simultaneously two time dependent mechanical and thermodynamical sources of nonequilibrium.

2. The model

We consider a one dimensional array of atoms, harmonically and bidirectionally coupled. The chain is divided in two segments (L, R) with different coupling intensities K_L and K_R between elements and coupled together also harmonically with a coupling constant K_{int}. The system is subject to an on-site potential (Frenkel–Kontorova (FK) chains) as it is shown in Fig. 1.

The Hamiltonian of the system can be written as: $H = H_L + H_{int} + H_R$ where $H_{L/R}$ is the Hamiltonian to the left (L)/right (R) segments respectively and H_{int} represents the interaction between the two segments.

$$H_{L/R} = \sum_{i=1}^{N} \frac{P_i^2}{2m_i} + \frac{1}{2}K_{L/R}(X_{i+1} - X_i)^2 - \frac{V_o}{4\pi^2}\cos(2\pi X_i) \tag{1}$$

with N the total number of atoms.

If each segment has $N/2$ elements, the interaction Hamiltonian can be written as:

$$H_{int} = \frac{1}{2}K_{int}(t)(X_{N/2+1} - X_{N/2})^2 \tag{2}$$

with m_i the mass of the ith atom, $X_i = q_i - ia$ denotes the displacement from the equilibrium position ia, where a is the periodicity of the on-site potential (corresponding to a commensurate state), and P_i is the momentum.

$K_{L/R}$ are the elastics constants in each segments and V_0 is the depth of the on-site potential. The fixed ends of the L/R segments are in contact with two thermal baths which are simulated through Langevin type reservoirs with zero mean and variance $\langle \xi_i(t), \xi_k(t')\rangle = 2\gamma K_B T_i \delta(t - t')\delta_{i,j}$, where γ is the strength of the coupling between the system and the baths, and T_i, $i = L/R$, is the temperature of each bath. The system is driven out of equilibrium by two different mechanisms:

(a) Modulation of the coupling between segments: $K_{int}(t) = K_0(1 + \sin(\omega_K t))$.
(b) Modulation of the temperature of the reservoirs: $T_{L,R}(t) = T_{0,i}(1 + \Delta sgn(\sin(\omega_{temp} t)))$, $i = L, R$ with $T_{0,i}$ the reference temperature of each reservoir.

The integration of the equations of motion is performed with a 2nd-order stochastic Runge–Kutta algorithm, for sufficiently long time (of order of 10^9–10^{10} integration steps) to guarantee that the system reaches a stationary state. We apply fixed boundary conditions and for the numerical simulations we use dimensionless parameters: spring constants K_i in units of K_R, moments in units $[a(mk_R)^{1/2}]$, frequencies in units $[(K_R/m)^{1/2}]$ and temperatures in $[a^2 K_R/k_B]$. For a typical atom and a typical situation these units corresponds to frequencies $\sim 10^{13}$ s^{-1} and temperatures $\sim 10^3$, 10^4 K. Thus the nondimensional temperatures 0.01–0.1 correspond to temperatures of the order 100–1000 K. On the other hand, frequencies are assumed to be smaller than the inverse of typical electron–phonon relaxation times $\sim$0.1 ps (dephasing time), in order to consider only the relevant time scales of phonon scattering processes.

From the continuity equation, the energy current that flows to and from a particle should cancel each other when the system reaches the steady state, since there are not temporal variations of the mean local density of energy. The local time-dependent heat current is calculated as:

$$J_i(t) = K_i\dot{X}_i(t)[X_i(t) - X_{i-1}(t)]. \tag{3}$$

We define the net heat current in each segment $\bar{J}_{L,R}$ averaging over an integer number of periods after a transient time as:

$$J_{L/R} = \frac{1}{\tau}\int_0^\tau \bar{J}_i(t)\,\mathrm{d}t. \tag{4}$$

In the steady state $J_{L,R}$ are independent of the site in each segments. In the same way, the effective local temperature is defined as:

$$T_{eff}(i) = \frac{1}{\tau}\int_0^\tau \dot{X}_i(t)^2\,\mathrm{d}t. \tag{5}$$

On the other hand, conservation of total power implies that the power P invested by external agents into the system is dissipated into the reservoirs, therefore:

$$P = \dot{W} = \dot{Q}_R + \dot{Q}_L = J_R + J_L \tag{6}$$

where $\dot{Q}_L$ and $\dot{Q}_R$ are the rates of heat absorbed for the reservoir L and R respectively (defined positive when heat flows into the reservoir), and $\dot{W}$ is the rate of work done in the contact.

3. Results

We study the effect of two sources of nonequilibrium in the system. As a first step, we control the coupling between segments through a time dependent modulation of the intensity. Then, we incorporate a time modulation of the temperature of the reservoirs and we analyze the cooperative effect of both drivings on the heat transport.

3.1. Single resonant transport

In order to study the response of the system to the modulation of the contact, we depict in Fig. 2 the current through the L and R segments as a function of ω_K. We observe different regimes, corresponding to regions I, II, III and IV in Fig. 2. We choose arbitrary and without loss of generality $T_L > T_R$ because discussion does not change qualitatively.

In region I, $J_R = -J_L > 0$, heat transport is mainly dominated by the gradient of temperature (heat current is defined positive when heat flows into the bath). The averaged net power released to the system is zero and the heat flows from hot to cold. Thus, when ω_K is very low (adiabatic driving limit), the system reduces to two coupled segments with a coupling constant $K_0/2$.

In region II the heat still flows from hot to cold but with different absolute values in each segment because of a net contribution due to the power released to the system, that according to Eq. (6) means $J_R - |J_L| = P > 0$, with $J_L < 0$.

The separatrix between region II and III corresponds to a frequency for which the heat current in the left segment is zero. This is the onset of regime III where a current inversion in the L segment occurs. The energy transport is mainly dominated by the power released in the contact region and dissipated into both reservoirs. Energy currents take different absolute values in both segments due to asymmetry. There is a frequency for which the power released to the system ($J_R + J_L$), always positive, achieves a maximum value as it is expected for a resonant behavior and depends on the eigenfrequency spectral distribution of the system. This phenomenon is found to be robust for different temperatures and direction of the gradients. Moreover, it is found even in the absence of thermal bias ($T_{R,0} = T_{L,0}$, not shown here), indicating that this is mainly a "pumped energy" regime dominated by a phonon pump contribution to the heat current due to a work done on the system.

The temperature profile exhibits a discontinuity at the interface (see Fig. 3), except in region III. For region I and II a negative-value slope temperature profile in L segment indicates a heat flow from L reservoir as it is shown in Fig. 2. The crossover to region III occurs for a zero-value slope, thus indicating that a current reversal occurs.

In region IV the contribution due to the gradient of temperature is again the dominant one and the power released is almost zero. The current here corresponds to a regime with a coupling intensity oscillating very fast ($\omega_K \to \infty$), converging to a time average constant value K_0.

In order to have a qualitative insight of the underlying physical mechanism of the observed rectification and inversion phenomena, we show in Fig. 4 the phonon spectrum ($K_0 \ll K_L, K_R$) of the interface particles at the left and right side of the contact for different driving frequencies ω_K regimes. The spectrum is presented for an arbitrary direction of the temperature gradient ($T_L > T_R$) because the phonon bands behavior do not change significantly when the temperature gradient is reversed.

The match or mismatch of the spectrum of the two particles controls the energy (phononic) current through the contact and along the device. As the power supply ($\sim\omega_K^2$) at the interface affects the kinetic energy of the particles, it is expected

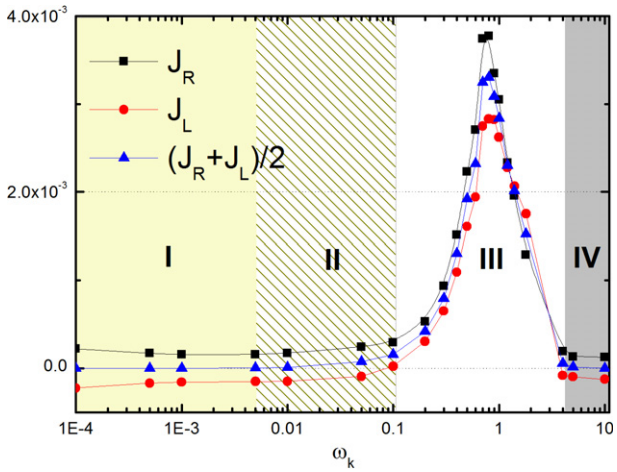

Fig. 2. Heat flux *vs* ω_K. J_L (black square) is the energy current through the left segment and J_R (red circle) in the right segment. $J_R + J_L$ (up blue triangle) is the power released into the system. Regions I–IV are discussed in the text. Parameters (in dimensionless units): $V_0 = 5$, $\gamma = 0.5$, $\Delta = 0.5$, $K_L = 2K_R = 1$, $K_0 = 0.05$, $\omega_{temp} = 10^{-4}$, $T_{0,L} = 0.15$, $T_{0,R} = 0.05$, $N = 30$.

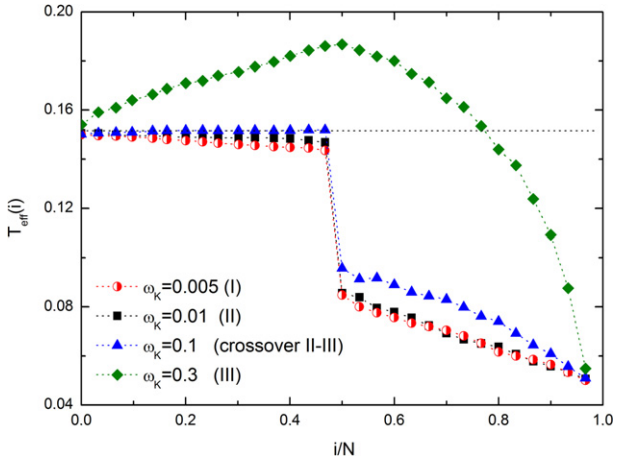

Fig. 3. The effective temperature profiles for four selected ω_K values of Fig. 2.

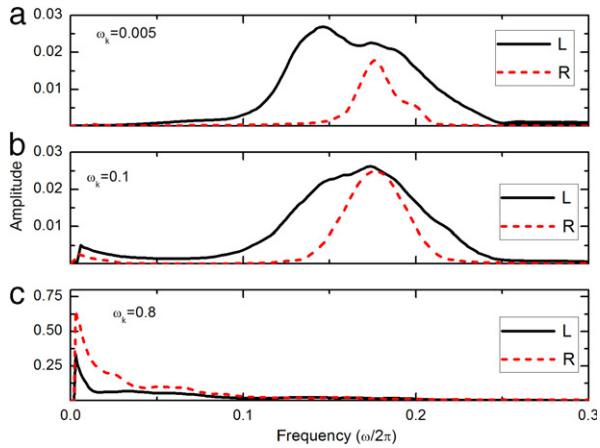

Fig. 4. Single-particle frequency spectrum of the particles to the left (L, solid line) and right (R, dashed line) of the interface. From top to bottom: $\omega_K = 0.005, 0.1, 0.8$. Parameters as in Fig. 2.

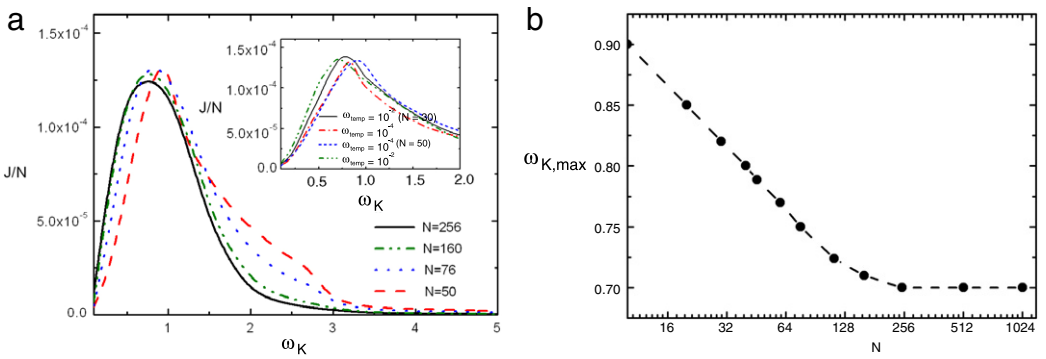

Fig. 5. Left (a): J/N vs ω_K for different N. Red line corresponds to $N = 50$, blue line to $N = 76$, green line to $N = 160$ and black one to $N = 256$. Inset: J/N vs ω_K for different $\omega_{temp} = 10^{-2}$, 10^{-4} and $N = 30$, 50. Right (b): Optimal $\omega_{K,max}$ *vs* N. $\omega_{temp} = 5 \cdot 10^{-4}$. (For interpretation of the references to color in this figure legend, the reader is referred to the web version of this article.)

that ω_K will play a relevant role on the behavior on the phonon bands shifts as that produced by thermal excitations on the phonon bands of the standard *FK* model. For ω_K in regions I–II (Fig. 2) the non-linear on-site potential plays a fundamental role confining the particles near their equilibrium positions, the valleys, thus a low-frequency band-gap is opened (Fig. 4(a)). By linearizing the FK equations of motion one can easily obtain the phonon band, $\sqrt{V_0} < \omega < \sqrt{V_0 + 4k_i}$ [27]. Transition from region II to III is a crossover where the height of the non linear on-site potential is of the order of the local thermal energy of the particles (due to injected energy) so the low frequency part of the phonon bands starts to be populated. For ω_K in region III the particles have large enough kinetic energies to overcome the wells of the potential and the low frequency part of the spectrum becomes more important (Fig. 4(b)) in the phonon bands of the L and R segments. In Fig. 4(c) the on-site potential becomes negligible, the FK model degenerates to a harmonic one with $0 < \omega < 2\sqrt{k_i}$ phonon bands with mainly noninteracting phonons. The interface works as a scatter point for high frequency phonons but not for low frequency ones. These soft modes (including zero-mode) have bigger mean free path thus playing a fundamental role in the energy conduction.

Heat transport is mediated mainly by low frequency acoustic phonons. The role of the on-site potential is to produce a shift in the minimum cutoff frequency from zero to V_0. Due to the driving, this minimum cutoff can also be decreased, so more low frequency phonons are involved in the transport process increasing the heat current. In this way we can control and tune the heat transfer *dynamically*, overlapping the phonon bands in the low part of the spectrum. We also find that this behavior of the phonon bands is robust against changes in the directions of temperature gradients.

Another interesting feature to investigate is the size system effect on the energy transport, which becomes relevant from a practical point of view, in order to control heat in different scale systems. We find that the resonance behavior is robust for all values of N, that is not a size effect. In Fig. 5(a) we show the heat current normalized to the length of the chain for the L segment as a function of ω_K for different values of N. We define $\omega_{K,max}$ as the optimal driving frequency for which J is maximum. We observe that the position of the peaks shifts to lower frequencies when N increases. In Fig. 5(b) we plot $\omega_{K,max}$ as a function of the size N for the L segment. This "red shift" effect is veiled when the size increase. This means that in practice we can obtain lower optimum driving frequencies by enlarging the system. The heat conduction in the FK lattice follows Fourier's law when the system size is large enough. That is the response time τ that characterized the time scale for the energy to diffuse along the system is proportional to N^2. However in our case $\omega_{K,max}$ does not follow that proportionality. On the other hand, for small N, $\omega_{K,max}$ is neither proportional to N^{-1} as should be expect for a pure ballistic transport of phonons. So, in the resonant regime typical time scales are not proportional to N^1 or N^2 (not purely ballistic or diffusive) due to the presence of driving and nonlinearity.

3.1.1. Multiple resonant transport

As a second step, we analyze the energy transport when two independent time dependent sources of nonequilibrium are driving the system. We introduce a periodic time modulation of the temperature of both reservoirs with frequency ω_{temp}, for a fixed temperature bias: $T_{L,R}(t) = T_{0,i}(1 + \Delta sgn(\sin(\omega_{temp} t)))$ $i = L, R$

In Fig. 6 we plot the current J_R vs ω_{temp} for the case $T_L > T_R$ (this election is arbitrary and do not affect the analysis).

When ω_K goes to zero (so $K_{int} \approx cte$) and in the adiabatic limit ($\omega_{temp} \to 0$), the ends of the chain feel the constant temperatures $T_{L,0}$ and $T_{R,0}$. On the other side, in the fast-oscillating limit $\omega_{temp} \to \infty$, the baths are driven so fast that the two ends of the chains cannot respond accordingly, thus the system only feels the time average temperatures $T_{L,0}$ and $T_{R,0}$. In both cases $|J_R| = |J_L|$. As long ω_{temp} is increased from zero, the heat current shows a decreasing behavior. However, beyond a critical value ($\omega_{temp} \approx 0.01$ in Fig. 6) the current becomes ω_{temp} independent. This can be understood from the discontinuity in the effective local temperature $T_{eff}(i)$ profile at the interface, shown in Fig. 7. For slow coupling modulation of the baths, the temperature gradient in the right segment is greater, so the heat current. When ω_{temp} is increased the temperature gradient gets smaller and the heat current decreases, tending to a limit temperature profile. This indicates a regime where

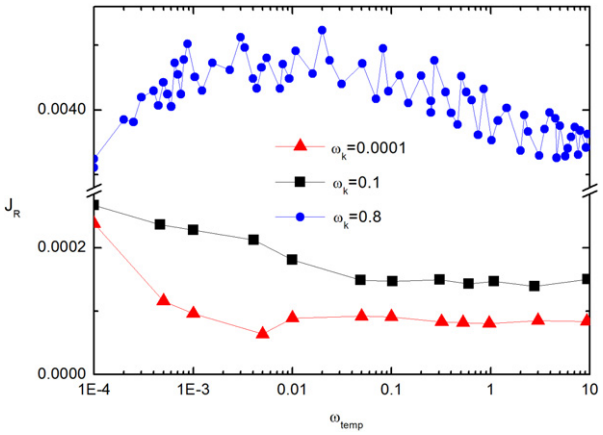

Fig. 6. J_R *vs* ω_{temp} for $\omega_K = 0.8, 0.1, 10^{-4}$.

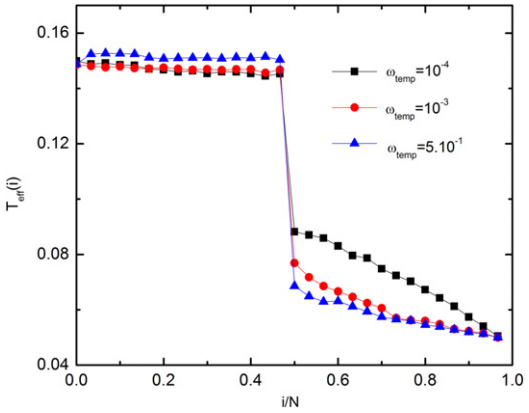

Fig. 7. Local effective temperature $T_{eff}(i)$ *vs* site number for $\omega_{temp} = 10^{-4}$, 10^{-3} and $5 \cdot 10^{-1}$ and $\omega_K = 10^{-4}$. Parameters as in Fig. 2.

the current is almost ω_{temp} independent with a value mainly determined by the low frequency coupling modulation ω_K (Fig. 6). Otherwise, in the left segment the temperature gradient is almost zero, thus it acts mainly as an insulator.

On the other hand, for values of ω_K in the resonant region III of Fig. 2(a) we observe a qualitatively change in J_R (as J_L also) curves when ω_{temp} changes (see Fig. 6). A multiresonance response appears *but* depending on ω_{temp}. In Fig. 8(a) we show the curves for $\omega_K = 0.4, 0.8$. The values of J_R are "confined" in between two envelopes. In Fig. 8(b) we plot the maximum "distance" (ΔJ_{max}) between the upper and lower envelopes as a function of ω_K observing that this magnitude presents a single resonant response.

Let us examine the reason for the appearance of multiresonant peaks. The presence of multiple peaks is related to the eigenfrequency structure of the on-site harmonic system, becoming more dense as N increases. As it is shown if Fig. 9 the positions of the peaks for the harmonic and FK models seem to be close, but not identical, suggesting a similar resonant mechanism [24]. However, the current is smaller in the FK system because of phonon scattering processes due to anharmonicity.

When ω_K moves away from $\omega_{K,max}$ the on-site potential becomes more relevant. The multiresonance response is still found, but with upper and lower envelopes getting closer, as it is depicts in Fig. 8(a). Thus the role of the non linear on-site potential is to smooth the multiresonant peaks. The mechanism for a single peak should be still explained by the fact that the external frequency due to driving is resonant with a characteristic frequency of the system, but with an upper envelope tending to the lower one. In this way we can observe the lower envelope with a single resonant peak as in Fig. 2.

In Ref. [24] it was found a multiresonance behavior due to the action of an external driving. However, here we present a richer and complex feature of this phenomenon, that emerges when two time dependent sources of nonequilibrium act in a synergetic way on the system. From Figs. 2 and 8(a) we observe a multiresonant response that requires not only a driving of K_{int}, but also a modulation of the temperature of the reservoirs.

The above discussion reveals clearly the presence of two distinct regimes depending on the two relevant frequencies, and a crossover between them: a "thermal" transport regime dominated by the temperature gradient and one dominated by the power released into the system by the mechanical driving. See Fig. 9.

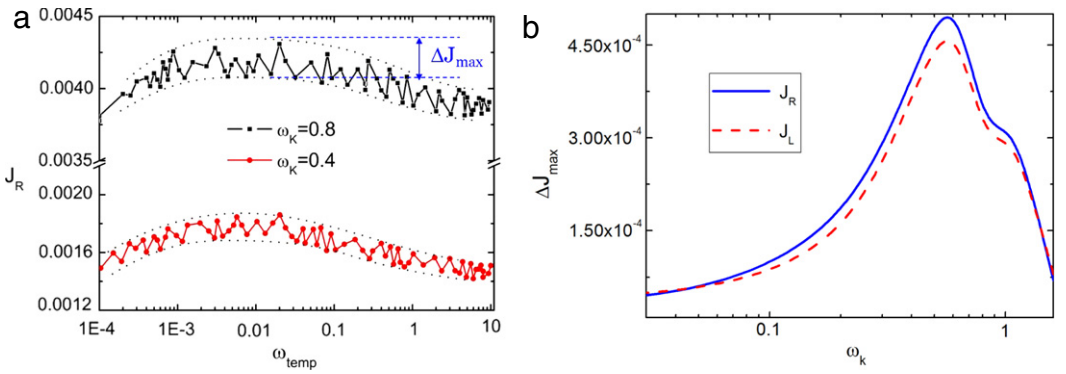

Fig. 8. Left (a): J_R *vs* ω_{temp} for two ω_K values in the single resonant regime. Dotted lines indicate the approximate upper and lower envelope curves. Right (b): Distance between envelopes *vs* ω_K.

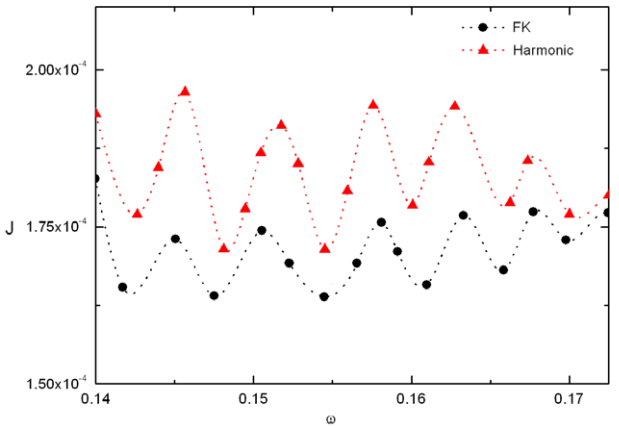

Fig. 9. Comparison of the harmonic case and the FK case in a randomly selected frequency region. Heat current vs driven frequency ω_K for $\omega_{temp} = 5 \cdot 10^{-4}$ and $T_{L,0} = T_{R,0}$.

4. Concluding remarks

In summary, we studied the heat transfer along a one dimensional system formed by two *FK* segments in contact and with their ends coupled to thermal reservoirs with modulated temperatures. The coupling between segments is also time modulated and provides a source of energy (work) delivered into the system. We mainly focused our analysis in the heat transfer along the system for a broad range of the two involved frequencies and the most characteristic regimes. Keeping fixed the average temperatures of the thermal baths, we found a range of coupling frequencies for which the system presents a single resonance response for the heat flux. For slow and fast coupling modulations this phenomenon vanishes and the heat current takes smaller values than in the resonant regime. We also showed that there exists a robust current reversal in one of the segments.

On the other hand, when both time dependent nonequilibrium sources act simultaneously, we found two different responses as a function of ω_{temp}. One corresponding to a resonant regime with the presence of multiple peaks for frequencies related to the eigenfrequencies of the system that are bounded by the number of oscillators. This regime is found in the window where the system presents a "pumped energy" regime for ω_K. The curves are bounded by envelopes getting closer as long the frequency moves away from the optimal ω_K. The other regime corresponds to a non resonant response where the heat current takes a constant value as long as the frequency of the temperature modulation increases.

We also found a "red shift" for the single resonant frequency $\omega_{K,max}$ which is a size effect. In Ref. [28] it was found that a characteristic frequency is red shifted varying the system size when the temperature of the thermal baths is time modulated. On the other hand, it was shown in Ref. [26] that when the temperature of the reservoirs are kept constant, but an external driving is applied, the characteristic resonant frequency is not size dependent. However, our results suggest that this effect depends on the mechanical and the thermodynamical dynamical contributions acting altogether. As it is expected, when the mechanical driving is present but without temperature there is not a heat current (trivial case not shown here). With temperature and for a fixed ω_K, we also find a frequency shift that depends on ω_{temp} and N, as it is show in the inset of 5(a). However a detailed analysis of how this cooperative effect depends on the size of the system deserves further investigation in a future work.

The nondimensional parameters used here correspond to typical values that can be realized experimentally. Thus the comprehension of this cooperative resonant phenomena will allow to achieve a better mechanical and thermodynamical control of the energy transport in order to design devices whose features help to improve the energy transfer in low dimensional systems.

Acknowledgment

M.F.C. is supported by Conicet-PIP D-3189/2012.

References

[1] N, Li, J, Ren, L, Wang, G, Zhang, P, Hänggi, B, Li, Rev. Modern Phys. 84 (3) (2012) 1045.
[2] E.C. Cuansing, H. Li, J.S. Wang, Phys. Rev. E 86 (2012) 031132.
[3] L.S. Cao, R.W. Peng, Mu Wang, Appl. Phys. Lett. 84 (2008) 011908.
[4] E. Pereira, Physica A 390 (23–24) (2011) 4131–4143.
[5] S. Liu, X.F. Xu, R.G. Xie, G. Zhang, B.W. Li, Eur. Phys. J. B 85 (2012) 337.
[6] L. Wang, B. Hu, B. Li, Phys. Rev. E 88 (2013) 052112.
[7] L. Wang, B. Hu, B. Li, Phys. Rev. E 86 (2012) 040101(R).
[8] S.G. Das, A. Dhar, O. Narayan, J. Stat. Phys. 154 (2014) 204–213.
[9] A.V. Savin, Y.A. Kosevich, Phys. Rev. E 89 (2014) 032102.
[10] B. Hu, L. Yang, Physica A 372 (2) (2006) 272–278.
[11] C.A. Polanco, A.W. Ghosh, J. Appl. Phys. 116 (2014) 083503.
[12] L. Wang, B. Hu, B. Li, Phys. Rev. Lett. 88 (2002) 094302.
[13] B. Li, L. Wang, G. Casati, Phys. Rev. Lett. 93 (2004) 184301.
[14] B. Li, LJ. Lan, L. Wang, Phys. Rev. Lett. 95 (2005) 104302.
[15] C.W. Chang, D. Okawa, A. Majumdar, A. Zettl, Science 314 (2006) 1121.
[16] L. Wang, J. Wu, Phys. Rev. E 89 (2014) 012119.
[17] B. Li, L. Wang, G. Casati, Appl. Phys. Lett. 88 (2006) 143501.
[18] L. Wang, B. Li, Phys. Rev. Lett. 99 (2007) 177208.
[19] L. Wang, B. Li, Phys. Rev. Lett. 101 (2008) 267203.
[20] R. Xie, C.T. Bui, B. Varghese, Q. Zhang, C.H. Sow, B. Li, J.T.L. Thong, Adv. Funct. Mater. 21 (2011) 1602.
[21] N. Li, F. Zhan, P. Hänggi, B. Li, Europhys. Lett. 80 (2009) 011125.
[22] L. Arrachea, E.R. Mucciolo, C. Chamon, R.B. Capaz, Phys. Rev. B 86 (2012) 125424;
C. Chamon, E.R. Mucciolo, L. Arrachea, R.B. Capaz, Phys. Rev. Lett. 135504 (2011).
[23] B.K. Agarwalla, J.S. Wang, B. Li, Phys. Rev. E 84 (2011) 041115.
[24] S. Zhang, J. Ren, B. Li, Phys. Rev. E. 84 (2011) 031122;
J. Ren, B. Li, Phys. Rev. E 81 (2010) 021111.
[25] E. Cuansing, J.S. Wang, Phys. Rev. B 81 (2010) 052302;
E. Cuansing, J.S. Wang, Phys. Rev. E 82 (2010) 021116.
[26] B.Q. Ai, D. He, B. Hu, Phys. Rev. E 81 (2010) 031124.
[27] B. Li, J.H. Lan, L. Wang, Phys. Rev. Lett. 95 (2005) 104302.
[28] N. Li, P. Hänggi, B. Li, Europhys. Lett. 84 (2008) 40009.